Profiling of Saharan dust from the Caribbean to West Africa, Part 1: Layering structures and optical properties from shipborne polarization/Raman lidar observations

Franziska Rittmeister[1], Albert Ansmann[1], Ronny Engelmann[1], Annett Skupin[1], Holger Baars[1], Thomas Kanitz[2], and Stefan Kinne[3]

[1]Leibniz Institute for Tropospheric Research, Leipzig, Germany
[2]ESTEC, Noordwijk, The Netherlands
[3]Max Planck Institute for Meteorology, Hamburg, Germany

Correspondence to: A. Ansmann (albert@tropos.de)

Abstract. Multiwavelength polarization/Raman lidar observations of the Saharan air layer (SAL) were performed aboard the German research vessel R/V Meteor during a one-month transatlantic cruise from Guadeloupe to Cabo Verde over 4500 km from 61.5°W to 20°W in April-May 2013. The shipborne lidar measurements are part of SALTRACE (Saharan Aerosol Long-range Transport and Aerosol-Cloud Interaction Experiment). Four observational cases representing key stages of the SAL evolution between Africa and the Caribbean are studied in detail in terms of layering structures and optical properties of the mixture of predominantly dust and aged smoke in the SAL. We discuss to what extend the lidar results confirm the validity of the SAL conceptual model which describes the dust long-range transport and removal processes over the tropical Atlantic. Our observation of a rather clean marine aerosol layer (MAL) suggests that the removal of dust from the MAL, located below the SAL, seems to be very efficient over the remote tropical Atlantic (more than expected by the model) and/or that the removal of dust from the SAL by gravitational settling is weaker than expected. To explain the observed homogenous (height-independent) dust optical properties from SAL base to SAL top and from the African coast to the Caribbean, we have to assume that the particle sedimentation strength is in fact reduced and dust vertical mixing and upward transport mechanisms must be active in the SAL. Based on lidar observations in 20 nights in May 2013, we found, on average, SAL and MAL layer mean values (at 532 nm) of the extinction-to-backscatter ratio (lidar ratio) of 17±5 sr (dust-free MAL) and 43±8 sr (SAL), of the particle linear depolarization ratio of 0.025±0.015 (MAL) and 0.19±0.09 (SAL), of the particle extinction coefficient of 67±45 Mm^{-1} (MAL) and 68±37 Mm^{-1} (SAL). The 532 nm optical depth of the lofted SAL was found to be, on average, 0.15±0.13 during the ship cruise. The comparably low values of the SAL mean lidar ratio and depolarization ratio (compared to pure dust values of 50–60 sr and 0.3, respectively) indicate a smoke contribution to light extinction of the order of 20% during May 2013, at the end of the burning season in central-western Africa.

1 Introduction

Dust particles can travel over long distances of more than 10000 km in the free troposphere (Haarig et al., 2017a) and can be lifted up to the tropopause during long-range transport (Mamouri and Ansmann, 2015; Hofer et al., 2016, 2017). Dust is an important component of the northern hemispheric aerosol system and sensitively influences environmental and climatic conditions on the regional to intercontinental scale (Myhre and Stordal, 2001; Sokolik et al., 2001; Tegen, 2003; Balkanski et al., 2007). The impact of mineral dust on the evolution and lifetime of liquid-water, mixed-phase, and ice clouds via heterogenous ice formation is presently in the focus of atmospheric research (Seifert et al., 2010; Murray et al., 2012; Hoose and Möhler, 2012; Atkinson et al., 2013; Phillips et al., 2013; DeMott et al., 2015; Kiselev et al., 2017).

The Saharan desert is the world's largest mineral dust source (Prospero et al., 2002; Cakmur et. al., 2006; Huneeus et al., 2011) and the transport of mineral dust across the tropical Atlantic is the most prominent example of a powerful long-distance transport of mineral dust. Karyampudi et al. (1999) presented a conceptual model to describe the transport and deposition of dust during advection from Africa to America. We introduce this conceptual model in Sect. 1.1. Dust advection across the tropical Atlantic during the summer months is almost not affected by anthropogenic pollution so that changes in the dust characteristics during transport can be studied in large detail. The pioneering work of J. Prospero (Prospero, 1968; Prospero et al., 1972), which he began more than 50 years ago at Barbados in August 1965, triggered numerous dust research activities and well organized field campaigns in western Africa and over the tropical Atlantic. Overviews of these advanced field campaigns conducted during the last 15 years are given in Ansmann et al. (2011) and Ryder et al. (2015).

To investigate dust and its climate-relevant aspects comprehensive dust field experiments (ground-based and airborne activities, in situ measurements combined with active and passive remote sensing) are required with focus on the complex relationship between the microphysical, chemical, morphological shape, optical, radiative, and cloud-process-relevant properties of dust particles. The latest attempt to characterize dust over scales of several thousands of kilometers of travel distance (equivalent to 5-10 days of travel time) has been performed by the series of well-defined field activities: The Saharan Mineral Dust Experiments SAMUM-1 (southern Morocco, summer 2006) (Heintzenberg, 2009) and SAMUM-2 (Cabo Verde, in the winter and summer of 2008) (Ansmann et al., 2011), and the Saharan Aerosol Long-Range Transport and Aerosol-Cloud-Interaction Experiment SALTRACE (Barbados, in the summers of 2013 and 2014, and the winter of 2014) (Weinzierl et al., 2017).

Winter as well as summer-mode dust transport regimes (Schepanski et al., 2009; Ben-Ami et al., 2009) were covered by the two SAMUM-2 and three SALTRACE field phases (Tesche et al., 2011a; Haarig et al., 2017a). Based on the SAMUM-2 observations and simultaneously performed lidar measurements in Amazonia it was clearly demonstrated for the first time that not only desert dust, but also significant amounts of biomass burning smoke are transported towards South America (Ansmann et al., 2009; Tesche et al., 2011b; Baars et al., 2011) and even sporadically to the Caribbean during the winter half year (Haarig et al., 2016). The dust/smoke layers are advected at comparably low heights, typically below 3 km height, during the winter season. In contrast, almost pure dust plumes leave the African continent in summer. The dust layers reach up to 5-6 km height over western Africa (Tesche et al., 2011a) and the eastern part of the tropical Atlantic in summer. The dust is then found over Barbados between about 1.5 km and 4 km height (Groß et al., 2015; Haarig et al., 2016, 2017a).

The main goal of the SAMUM and SALTRACE activities was to conduct a detailed vertically resolved characterization of Saharan dust close to the source as well as within the Saharan air layer (SAL) on the way towards the Caribbean, more than 5000 km downwind the main source regions. Well designed efforts of combined airborne and ground-based in situ aerosol observations and remote sensing were realized during all of the three campaigns. To better link the SAMUM and SALTRACE

5 results, continuous lidar observations were conducted aboard the German research vessel R/V Meteor during a cruise from Guadeloupe to Cabo Verde from 29 April to 23 May 2013, and thus during the transition period from winter to summer dust transport conditions. The SAMUM and SALTRACE field sites (Morocco, Cabo Verde, Barbados) and the R/V Meteor cruise are shown in Fig. 1 (top).

The fully automated multiwavelength polarization/Raman lidar (Engelmann et al., 2016) aboard the research vessel mea-

10 sured height profiles of optical and microphysical properties of the particles in the marine aerosol layer (MAL) and of the mixture of predominantly dust and smoke in the SAL on top of the MAL. Kanitz et al. (2014) provided a first overview of the shipborne lidar observations across the Atlantic, discussed the general features of dust layering during the cruise, and compared the dust profile structures with preliminary dust modeling results. The authors also presented two contrasting cases (for very fresh and aged dust plumes) in terms of vertical profiles of particle backscatter and extinction coefficients, extinction-

15 to-backscatter or lidar ratio, linear depolarization ratio, and Ångström exponents (describing the wavelength dependence of backscatter and extinction).

In a series of two articles, we now present the final results of the cruise. In part 1, we discuss the dust layering characteristics in large detail (Sect. 3.2) and the aerosol optical properties of four cases (Sect. 3.3), which we denote as key stages of the SAL evolution across the Atlantic. We compare our R/V Meteor lidar observations with the main features of dust transport and

20 removal over the Atlantic Ocean as described by the conceptual model developed by Karyampudi et al. (1999) in Sects. 3.2.1 and 3.3.1. The conceptual model is explained in Sect. 1.1. We discuss the mixing state of dust and non-dust aerosol components in the SAL in Sect. 3.3. All available cloud-free nighttime Raman lidar observations (20 nights within the 1–23 May 2013 period) were analyzed and the vertical mean values of particle extinction, lidar ratio, and depolarization ratio for MAL and the lofted SAL were determined. These results are presented in Sect. 3.3 as well. In part 2 (Ansmann et al., 2017), the selected

25 four key observational cases are further analyzed by applying the Polarization Lidar Photometer Networking (POLIPHON) method of Mamouri and Ansmann (2017). Fine dust, coarse dust, and non-dust backscatter contributions are separated and dust, marine, and smoke/haze contributions to light extinction and particle mass concentration are quantified in part 2 and compared with respective dust forecasts of three well-established dust models.

1.1 Conceptual model

30 The conceptual model (Karyampudi et al., 1999) is an important contribution to the literature and describes the dust transport from Africa to North America in detail. According to this model, which is based on research performed in the 1970s to 1990s, hot, dry, dust-laden air masses emerge from the western coast of Africa as a series of large-scale pulses in the summer months. Associated with easterly wave activity, Saharan dust outbreaks occur as discrete episodic pulses, which generally last 3–5 days. These dust outbreaks are mostly confined to a deep, well-mixed layer, denoted as the Saharan air layer, SAL, that often extends

to 5–6 km in height over West Africa due to intense solar heating in summer months. The airborne dust is carried westward by the prevailing easterly flow in the latitude belt of 10°–25°N. As the dust plumes approach the West African coastline and are advected further west in the predominantly easterly flow, the base of the SAL rises rapidly as it is undercut by the relatively clean northeasterly trade winds. The well-mixed SAL resides above the trade wind inversion layer which is on top of the humid and warm marine boundary layer, MBL, the top of which is normally capped by cumulus clouds. In the following, we define this layer from the ocean surface to the base of the SAL as the marine aerosol layer MAL. The observed optical properties clearly indicate that marine aerosol particles dominate the backscattering and extinction properties in the MAL. Another way to divide the vertical column up to SAL base (or the trade wind inversion) is related to cloud formation and occurrence. The layer up to the base of trade wind cumuli is called sub-cloud layer. The remaining layer from cloud base to SAL base or trade wind inversion is denoted as cloud layer (e.g., Siebert et al., 2013).

The dust transport takes usually 5-7 days across the Atlantic. While the SAL base rises with distance from Africa, the SAL top is assumed to lower due to the rapid depletion of giant particles away from the west African coastline and a general lowering of the dust-layer top, most likely induced by the subsidence associated with the Hadley circulation.

The strong temperature inversion at the base of the SAL limits convective activity and consequently precludes the possibility of strong wet removal (scavenging of dust particles below and within clouds and removal by wash and rain out), except during periods with deep convection and precipitation. The sub layers (in the MAL) receive dust particles by vertical downward mixing and mainly by gravitational setting (fallout) from the overlaying SAL. Convective mixing is pushing clean MBL air up in altitude and mass conservation forces dusty air to low altitudes, where it is efficiently removed by scavenging within and below clouds (rain out) or turbulent downward mixing. The residual aerosol layer located between the top of the convectively active MBL and the SAL possibly represents a mixture of mineral aerosol from the SAL above and sea salt aerosol from the MBL below. As the dust is advected west the low-lying material is eroded away by wet removal or dry deposition. Some of the low-lying dust may persist all the way across the ocean (Colarco et. al., 2003).

The question now arises: are these features of the dust transport across the Atlantic as described by the conceptual model in agreement with our shipborne lidar observations? Are there aspects that are not described and/or considered properly but have an impact on dust transport and removal? The discussion is presented in Sects. 3.2 and 3.3. Before we present the results in Sect. 3 , we briefly describe the R/V Meteor cruise, the lidar and other atmospheric measurement instruments used aboard the ship, and the basic lidar retrieval methods.

2   SALTRACE R/V Meteor cruise and instrumentation

The first vertically resolved lidar-based study of the SAL across the tropical Atlantic was presented by Karyampudi et al. (1999) based on the space lidar LITE (Lidar In-Space Technology) observation aboard the Space Shuttle Discovery in September 1994 (McCormick et al., 1993). Systematic studies of the east-to-west dust transport with the satellite lidar CALIOP were then presented by Liu et al. (2008a); Liu et al. (2008b). Further Saharan dust studies over the tropical Atlantic based on CALIOP measurements can be found in Adams et al. (2012) and Tsamalis et al. (2013). The latter authors characterized the decay of

the Saharan dust amount in terms of layer descent and deposition velocity. Both space lidars are so-called standard backscatter lidars. These lidar types allow a precise characterization of dust top and base heights and layering features, but do not permit an in-depth characterization of the dust optical properties as we present here based on the SALTRACE Meteor polarization/Raman lidar observations.

2.1 R/V Meteor cruise

The transatlantic cruise M96 of the German R/V Meteor took place from 29 April to 23 May 2013 starting at Guadeloupe ($16°$ N, $61°$ W) and ending at Cape Verde ($17°$ N, $25°$ W). The journey covered a distance of approximately 4500 km (Fig. 1, top). The containerized OCEANET-Atmosphere platform (Kanitz et al., 2011, 2013) aboard is usually operated during north-south cruises of R/V Polarstern between Bremerhaven, Germany, and Cape Town, South Africa, or Punta Arenas, Chile.

2.2 Polly[XT]

The multiwavelength Raman/polarization lidar system Polly[XT] (Engelmann et al., 2016) is the key instrument of the OCEANET-Atmosphere platform and installed inside the container. Polly stands for *POrtabLle Lidar sYstem*, XT for extend version. The lidar performed continuous observations during the four-week travel. By means of a two-telescope receiver arrangement for near-range and far-range tropospheric profiling, aerosol extinction profiles (computed from smoothed Raman signal profiles) are available from 400 m height up to cirrus and tropopause level and thus cover the upper part of MBL, most of the MAL and the entire SAL vertical range. Full overlap of the near–field telescope receiver field-of-view with the laser beam is at about 200-250 m. However, the full set of lidar products allow us to study the vertical distribution of dust and marine aerosol particles down to 100 m above sea level, because the determination of profiles of the backscatter coefficients and the depolarization ratio is based on the analysis of profiles of signal ratios and these profiles are available with good accuracy down to very low heights because the overlap effect widely cancels out. The advanced aerosol lidar enabled us to measure profiles of the particle backscatter coefficients ($180°$ scattering coefficient) at 355, 532, and 1064 nm, particle extinction coefficient at 355 and 532 nm, the respective lidar ratios (extinction-to-backscatter ratios) as well as the particle linear depolarization ratio at 355 and 532 nm (Freudenthaler et al., 2009; Engelmann et al., 2016; Baars et al., 2016). A discussion of the uncertainties in the retrieval products is also given in these articles.

One of the most important lidar parameters in dust observations is the volume depolarization ratio. This quantity is almost directly measured. The volume linear depolarization ratio is obtained from the calibrated ratio of the cross-to-co-polarized backscatter signal (Freudenthaler et al., 2009). Co and cross denote the planes of polarization (for which the receiver channels are sensitive) parallel and orthogonal to the plane of linear polarization of the transmitted laser pulses, respectively. The volume depolarization ratio is influenced by light depolarization by air molecules and aerosol and cloud particles. To obtain the particle depolarization ratio a correction for Rayleigh depolarization effects has to be applied (Freudenthaler et al., 2009).

The particle depolarization ratio is the most important parameter in the analysis of the aerosol mixing state and allows us to separate fine dust (dust particles with diameters <1 μm), coarse dust (super micron particles), and the non-dust aerosol components (Mamouri and Ansmann, 2014, 2017). The aerosol separation technique is based on characteristic particle linear

depolarization ratios for spherical marine aerosols, 0.02–0.03, for urban haze and biomass burning smoke, ≤ 0.05, and about 0.3 for desert dust at 532 nm (Sugimoto et al., 2003; Shimizu et al., 2004; Tesche et al., 2009). The corresponding analysis of the R/V Meteor lidar observations is given in the follow-up article (Ansmann et al., 2017).

Part of the results on the aerosol mixing state in the SAL are already discussed here in part 1 so that the following points need to be mentioned. In discussion, frequently the question arises to what extend dust aging effects by chemical treatments and cloud processes during long-range transport affect the accuracy of the dust separation technique. The assumption of a universal dust depolarization ratio of about 0.3 may not be generally valid. Aging of dust particles caused by cloud processing or chemical reactions on the dust particle surface (Abdelkadar et al., 2015, 2017) may change the chemical composition and shape characteristics (towards more smoothed, less irregular shapes) and thus may lead to a significant decrease of the dust depolarization ratio. However, the literature published on dust optical properties does not support such an aging effect as a function of transport time (Denjean et al., 2015; Haarig et al., 2017a; Hofer et al., 2016, 2017). Lidar observations always show maximum (pure dust) particle depolarization ratios of 0.28–0.35 disregarding the distance from the dust sources. A more reasonable argument for a possible decrease of the depolarization ratio is related to gravitational settling, which in principle should lead to a faster removal of coarse dust particles compared to fine dust particles (with diameters $<1\ \mu$m). Fine dust causes particle linear depolarization ratios of 0.14–0.18 at 532 nm, whereas the dust coarse mode after long-range transport leads to values between 0.35–0.4 (see discussion in Mamouri and Ansmann, 2017). A shift of the particle size distribution towards smaller particles should be reflected in a decreasing particle depolarization ratio. A small (minor) change of the depolarization ratio towards lower values was noticed in the SALTRACE summer measurements at Barbados (Haarig et al., 2017a). This trend was small and within the standard deviation covering the retrieval uncertainties and atmospheric variability. This small decrease may even be related to a slightly increasing impact of marine particles on the depolarization ratio in the SAL with increasing distance from Africa.

2.3   Sun photometer

The lidar profile observations were accompanied by sun photometer measurements in the framework of the Maritime Aerosol Network (MAN) as part of the Aerosol Robotic Network (AERONET) (Smirnov et al., 2009). The MICROTOPS II measurements provide column-integrated aerosol optical properties at 440, 500, 675, 870, and 936 nm (MAN, 2016). In this work, we will use the 440-870 nm Ångström exponent and 500 nm aerosol optical thickness (AOT). AOT uncertainties are around ± 0.02 for each AOT channel.

2.4   Auxiliary observations and data

Radiosondes for measuring temperature, humidity, and wind profiles were regularly launched at noon and midnight UTC by the German Weather Service on board the ship (AWI, 2016). The temperature and pressure profiles are used to compute the Rayleigh backscattering and extinction contributions to the observed lidar return signals. Missing radiosonde information has been filled with GDAS (Global Data Assimilation System) height profiles of temperature and pressure from the National Weather Service's National Centers for Environmental Prediction (NCEP) (GDAS, 2016). Aerosol sources apportionment anal-

ysis has been supported by air mass transport computation with the NOAA (National Oceanic and Atmospheric Administration) HYSPLIT (HYbrid Single-Particle Lagrangian Integrated Trajectory) model (HYSPLIT, 2016) using GDAS meteorological data (Stein et al., 2015). The backward trajectories have been used in conjunction with maps of active fires as determined with MODIS (Moderate Resolution Imaging Spectroradiometer) on board the Terra and Aqua satellites (MODIS, 2016).

5 ## 3   Results

3.1   R/V Meteor cruise overview

Figure. 1 (center panel) provides an overview of dust layering during the R/V Meteor cruise between 2 May and 23 May 2013. The figure is taken from Kanitz et al. (2014). The Saharan air layer, SAL, reached from the top of the marine aerosol layer, MAL, to about 3–5 km height. The MAL top height is indicated by a white line in Fig. 1. In this marine layer, sea salt particles 10 are mainly responsible for the measured optical properties, dust was almost absent. The particle depolarization ratio was usually <0.05 in the MAL except for the observations close the African coast on 20-23 May 2013. In the SAL, on the other hand, the particle depolarization ratio was usually >0.15 and indicated the predominance of dust particles.

Figure 1 (bottom panel), also taken from Kanitz et al. (2014), provides an overview of the aerosol optical thickness (AOT) at 500 nm wavelength during the cruise. The daily mean 500 nm AOT ranged from about 0.05, which is indicative for clean 15 marine aerosol conditions, to 0.7 during a major dust outbreak, observed at Mindeloh, Cabo Verde, at the the end of the cruise (case 1). During times with lofted dust (gray-shaded areas in Fig. 1, bottom) the AOT was mostly between 0.1–0.3. In addition, the Ångström exponent calculated from sun photometer AOT measurements in the 440–870 nm spectral range is shown in Fig. 1 (bottom). The Ångström exponent for marine particles is typically between 0.3–0.7 and drops towards very low values (close to zero) when desert dust with a strong coarse-mode fraction is present.

20 Three phases of dust transport are visible in Fig.1 (center and bottom panels). Close to Africa, SAL base height is low and not well defined. The column Ångström exponent is very low and indicates the strong impact of dust on the aerosol optical properties. Then the MAL top height or SAL base height stabilizes with values from 0.7–1.7 km height (downwind, towards the Caribbean). The Ångström exponent increases to values around 0.3, which indicates the still strong impact of lofted dust on the observed optical properties. Finally, in phase 3, the Ångström exponent increases to values around 0.5-0.6 which is indicative 25 for the increasing influence of marine aerosol on the column optical properties. The dust impact decreases significantly for sites west of 45°W.

3.2   Case studies of aerosol layering

We selected four cases to study the evolution of the SAL and changes in the dust optical properties with increasing distance from Africa in detail. They are indicated by numbers 1–4 in Fig. 1. Figure 2 shows these four lidar observations representing 30 key stages of aerosol layering over the tropical Atlantic. Case 1 and case 4 were already shown by Kanitz et al. (2014). They provide insight into the optical properties of a fresh and very aged dust plume, respectively. According to the HYSPLIT

backward trajectories, discussed in Sect. 3.3, the aged dust plume observed on 5 May 2013 (case 4) traveled 9 days across the Atlantic before reaching the research vessel at 53°W. In contrast, the fresh dust plumes (case 1) crossed the shipborne lidar at Mindeloh, Cabo Verde, after approximately 1 day over the ocean. Cases 2 and 3 were then selected to have three cases (1, 2, and 3) with linearly increasing temporal distance from the African west coast (1, 3, and 5 days).

5   The most remarkable features in Fig. 2 is the sharp increase of the volume depolarization ratio at the base height of the SAL from <0.03 in the MAL (marine particles dominate the volume depolarization ratio and cause very low light depolarization) to >0.1 in the SAL where the strongly light-depolarizing dust particles dominate (see cases 2 and 3). Note also the steady increase of the vertical extent of the MAL with distance from Africa (cases 1–3). Another noticeable finding is the decrease of the SAL depth with distance from Africa. Both findings (increase of MAL depth, decrease of SAL depth) are predicted or

10   described by the conceptual model (see Sect. 1.1).

To better understand the observed aerosol layering structures and vertical exchange processes over the tropical ocean and to check the consistency with the conceptual model in Sect. 3.2.1, we introduced the three layers MBL, MAL, and SAL. The top of the MBL is determined from the range-corrected signal profiles (shown in the left panel) by using the gradient method (Baars et al., 2008). At the top of the convective and humid MBL, the range-corrected lidar signal usually drops significantly

15   even during cloud-free conditions. The dark blue layers below the SAL in the right panels of Fig. 2 indicate the MAL. The top of the MAL is defined by the strong increase of the volume depolarization ratio at the interface between MAL and SAL (e.g., at about 1 km height in case 2) and can thus easily be obtained from the lidar observations. The vertical extent of the MAL does not necessarily be equal to the depth of the MBL. This was the case on 9 May 2013 (case 3), when the MAL was much deeper than the MBL. In Fig. 2 (cases 2-4), the white spots in the left panels indicate trade wind cumuli which developed in

20   the upper part of the MBL.

As was often observed during fair weather conditions (during SALTRACE over Barbados, during SAMUM-2 over Cabo Verde), cumulus convection can intensify and then the vertical extent of the clouds can increase from 300-500 m to 1-2 km. At these conditions, stratocumulus fields tend to develop at the top of the cloud active zone (below the trade wind inversion). The clouds dissolve later on and leave behind a marine aerosol up to SAL base (or MAL top). Such a situation may have led

25   to the aerosol layering as observed on 9 May 2013 (case 3 in Fig. 2). A vertically deep, cloudless MAL is detected reaching to almost 2 km height, while the depth of the MBL was <1 km as the white cumulus cloud spots in the right panel of Fig. 2 for case 3 indicate. The upper part of the MAL, from MBL top to MAL top, may be interpreted as a residual marine boundary layer which developed during times (hours to days before the lidar observation) with strong cumulus convection and vertical mixing (upwind the R/V Meteor). This residual boundary layer was also mentioned in the conceptual model in Sect. 1.1 when

30   discussing the undercutting effect occurring below the trade wind inversion.

3.2.1   Conceptual model versus lidar observations (part 1)

To facilitate the comparison between the lidar observations in Fig. 2 and the dust layering features and deposition aspects as described in the conceptual model in Sect. 1.1, we show a sketch (Fig. 3) of the observed dust layering in Fig. 2. The sketch highlights the different layers MBL, MAL, and the SAL and indicates vertical exchange mechanisms such as gravitational

settling of dust in the SAL and turbulent downward mixing of dust in the layers below the SAL, and also illustrates the undercutting effect, i.e., advection of clean air from the Northeast, below the SAL base (below the trade wind inversion). In the SAL, the dust is transported from east to west.

Wet deposition during times with clouds and precipitation as well as dry deposition contribute to the dust removal from the MAL. We analyzed METEOSAT satellite observations for the potential impact of wet deposition (by strong cumulus development and precipitation formation) and found that, except for case 4, wet deposition by deep convection and associated rain can be excluded. However, fair weather cumulus convection and light precipitation always occurs over the tropical Atlantic and thus a certain contribution of wet deposition to dust removal must be always taken into account.

Our observations are to a large extent in good agreement with the conceptual model. As already mentioned in the foregoing subsection, the observed changes in the MAL top height (increase), SAL base height and top height (decrease) and SAL vertical extent (decrease) with distance from Africa are similar to the ones described in the conceptual model. The observed sharp increase of the volume depolarization ratio at the interface between MAL and SAL suggests that injection of particles from the MAL into the SAL over the open Atlantic is almost impossible. Furthermore, the rather low depolarization ratio from the ocean surface to MAL top suggests a fast and efficient removal of dust from the MAL. The conceptual model (see Sect. 1.1) expects a mixture of marine and dust particles in the upper part of the MAL (from MBL top to SAL base), and thus a less efficient removal of dust than observed. In addition, a likewise weak dust fall out from the SAL into the MAL may have also contributed to the fact that the dust amount in the MAL was so low in May 2013 (during the built up phase of the summer transport regime).

Less sharp, more smooth structures in the depolarization ratio at the MAL/SAL interface were observed over the western part of Barbados during the SALTRACE summer campaigns in June and July 2013 and 2014 (Groß et al., 2016; Haarig et al., 2017a). Heat island effects associated with an enhanced turbulent air flow and downward mixing over Barbados was probably responsible for the observed strong downward mixing of dust from the SAL into the MAL (Engelmann et al., 2011; Jähn et al., 2016).

Gravitational settling plays the dominant role in the downward transport of dust in the SAL over the open Atlantic according to the conceptual model. However, our detailed profile observations presented in Sect. 3.3 as well as the SALTRACE observations at Barbados in June and July 2013 and 2014 (Groß et al., 2015; Gasteiger et al., 2017; Haarig et al., 2017a) suggest that further processes in the SAL are active in addition and counteract sedimentation of dust particles. We will continue the discussion of this point in Sect. 3.3.1, after the introduction and detailed explanation of the optical properties in the next section.

3.3 SAL and MAL optical properties

In Fig. 4, the vertical profiles of the derived optical properties for cases 1–4 are presented. The basic lidar signals were averaged (over 20–75 minutes) and vertically smoothed with window lengths of 457 and 563 m to reduce the uncertainty in the products caused by signal noise. Therefore, sharp changes in the profile as visible in Fig. 2 at SAL base obtained with temporal and vertical resolution of 30 s and 7.5 m are considerably smoothed out in Fig. 4.

A strong dust outbreak was observed on 23 May at Cabo Verde (case 1). According to the backward trajectories in Fig. 5 the dust layers arrived at Mindeloh, Cabo Verde, after a short travel over the tropical Atlantic and accumulated dust over 3–4 days. None of the shown trajectories crossed areas with biomass burning during the last five days before arriving over R/V Meteor. The analysis of the lidar observation regarding the contribution of non-dust aerosol components such as marine particles, urban

5   haze, and fire smoke particles to the total particle backscatter and extinction profiles is given in part 2 (Ansmann et al., 2017) and indeed shows that the non-dust contribution to light extinction at 532 nm is low (of the order of 10%). The daily mean value of the AERONET Ångström exponent in Fig. 1 is rather low (0.1) which is typical for major dust outbreaks.

The backward trajectories for case 2 (15 May 2013, 00:00 UTC) indicate a significant impact of smoke in the upper half of the SAL, i.e., above 2 km height. The trajectory for the arrival height of 2.5 km crossed fire areas at heights well within

10   the continental boundary layer. Fire smoke uptake was possible during almost two days. The contribution of African smoke and haze to particle extinction at 532 nm reached values around 50% in the upper part of the SAL (Ansmann et al., 2017). Compared to case 1, the daily mean AERONET Ångström exponent shows slightly enhanced values of 0.3 which may be an indication for the presence of a mixture of dust and fine-mode particles of continental origin, but also shows the increasing influence of marine aerosols in the MAL on the AOT with decreasing distance from Africa.

15   The dust layer on 9-10 May (case 3) also contained smoke according to the backward trajectory for the SAL center height of 2.5 km. The respective air mass crossed fire places at heights within the boundary layer over Africa. As discussed below, and in detail in part 2 (Ansmann et al., 2017), the smoke-related light extinction contribution was roughly 20% in the SAL in this case.

The aged dust plume observed on 5 May (case 4) monotonically descended from heights above 4500 m over Africa to

20   1-2 km height at about 55 °W. The profile of the particle depolarization ratios in Fig. 4 (case 4) indicate a similar amount of non-dust aerosol in the SAL and a 20% contribution to light extinction, probably by continental aerosol pollution. The air masses crossed fire places 9–10 days before arrival over R/V Meteor.

As can be seen in Fig. 4, the particle extinction coefficients for 355 and 532 nm ranged from about 50-100 Mm^{-1} in the SAL over the remote Atlantic Ocean for the moderate dust outbreaks (cases 2–4). Values up to around 300 Mm^{-1} were found

25   in case 1. A systematic decrease of the SAL backscatter and extinction values with distance from Africa (1700–4300 km) is not obvious from cases 2–4. The found decrease of the SAL AOT is related to the decrease of the SAL vertical extent. The 500 nm AOT decreased from 0.7 (case 1), over 0.3 (case 2) and 0.18 (case 3) towards about 0.15 (case 4). If we subtract a mean marine AOT of around 0.05 and a smoke-haze contribution of 10% (case 1), 40–50% (case 2) and 20% (cases 3-4) to the SAL AOT, the pure dust AOT in the SAL was close to 0.6 (case 1), 0.15 (case 2), 0.1 (case 3), and 0.08 (case 4).

30   Dust-related particle extinction coefficients in the SAL of 40–80 Mm^{-1} in cases 2–4 and of up to 270 Mm^{-1} in case 1 point to dust mass concentrations of 65–130 μg m^{-3} and 450 μg m^{-3} when applying recently updated dust mass–to-extinction conversion factors (Mamouri and Ansmann, 2014, 2017). For freshly emitted dust (over Africa) with a rather low fine dust fraction the conversion factor and thus the estimated dust concentrations may be even 25–30% larger (Osborne et al., 2008). Such young dust plumes may have been observed on 23 May 2013 (case 1). Dust mass concentration profiles are discussed

35   and compared with respective model forecasts in part 2 (Ansmann et al., 2017).

The particle depolarization ratios of >0.25 (case 1), of mostly 0.2–0.23 (case 2, lower part of the SAL), and of about 0.2 (cases 3–4) in Fig. 4 indicate that >80% (case 1), about 65–75% (case(2), and around 65% (cases 3 and 4) of the total particle backscatter coefficient was caused by dust backscattering (Tesche et al., 2011b). These dust backscattering fractions together with the observed particle (dust + non dust) lidar ratios at 532 nm in the SAL of 50–60 sr (case 1, upper part of the SAL), around 60 sr (case 2, upper part of the SAL), and 40–50 sr (case 3 and case 4, at SAL center height, see Fig. 4) point to lidar ratios for non-dust particles of around 60 sr (cases 1 and 2) and 30 sr (cases 3 and 4). In this estimation, we assume that the dust lidar ratio is 50–60 sr for western Saharan dust (Groß et al., 2011; Tesche et al., 2011a) and the respective dust depolarization ratio is around 0.3 at 532 nm disregarding transport time and potential aging and gravitational settling effects (see discussion in Sect. 2.2).

A critical point in our lidar data analysis is the smoke contribution to backscattering and extinction. Müller et al. (2007a) showed that fire smoke particles grow during long-range transport by a number of reasons such as, e.g., gas-to-particle conversion of organic and inorganic vapors during transport, condensation of large organic molecules from the gas phase on existing particles, particle coagulation, photochemical and cloud-processing mechanisms, and hygroscopic growth (Müller et al., 2005; Nikonovas et al., 2015). The surface-area mean radius (denoted as effective radius) of the size distribution of fire smoke was found to increase by a factor of 3 within a travel time of a week, from 0.1–0.15 μm to 0.3–0.5 μm (Müller et al., 2007a). As a consequence, the extinction-to-backscatter ratio may decrease from, e.g., >60 sr to values <40 sr, as obviously observed with the shipborne lidar. In fact, lidar ratios around 30 sr were frequently observed at Leipzig, Germany, in outflow aerosol plumes from North America (Müller et al., 2007b), and at the Maldives in aerosol layers advected from rural areas with high biomass burning activity of central-southern India (Franke et al., 2003).

In the discussion of the non-dust contributions to the SAL backscatter and extinction coefficients, the influence of marine particles causing 532 nm lidar ratios of 20–25 sr (Groß et al., 2011; Dawson et al., 2015; Haarig et al., 2017b) cannot fully be ruled out. During periods with stronger trade wind cumulus convection, cloud tops may partly penetrate into SAL base and inject marine aerosol particles during the updraft phases. Another source for marine particles is related to sea breeze events at the African west coast associated with the potential injection of marine aerosol into the dust layer when the dust outbreak plumes move westward and cross the coastal areas of West Africa.

The simultaneous observations of depolarization ratios at 355 and 532 nm allow further interpretation of the SAL aerosol mixing state. The SAL depolarization ratios at 355 and 532 nm decreased with distance from Africa from maximum values close to 0.23 at 355 nm and 0.27 at 532 nm (case 1) to values around 0.2 at both wavelengths (cases 3 and 4). For comparison, maximum dust linear depolarization ratios with values close to 0.25 (355 nm) and around 0.3 (532 nm) were found during SAMUM-1 (Freudenthaler et al., 2009) and SAMUM-2 (Groß et al., 2011). The difference of about 0.05–0.075 between the 532 and 355 nm particle depolarization ratios in cases 1 and 2 decreases to ≈0.02 and almost zero with distance from Africa in cases 3 and 4, respectively. Strongly growing smoke particles can explain the decreasing wavelength dependence. As shown by Müller et al. (2007a) and Ansmann et al. (2009), the increase of mean smoke particle size during long-range travel decreases the Ånsgtröm exponent for aged smoke towards values characteristic for mineral dust. This means that the relative impact of

aged smoke on particle backscatter and extinction increases more strongly at 532 nm than at 355 nm with travel time, and as a consequence the depolarization ratio decreases more strongly at 532 nm than at 355 nm.

The backscatter and extinction-related Ångström exponents in the SAL in Fig. 4 are typical for aerosols dominated by desert dust. The Ångström exponent (Ångström, 1964) was originally introduced to describes the wavelength dependence of AOT. In the lidar community, the Ångström exponent is also used to characterize the wavelength dependence of particle backscatter and extinction coefficients. Low values around zero for the short wavelength range from 355–532 nm within the SAL are in agreement with the SAMUM-2 observations (Cabo Verde, summer 2008, Tesche et al., 2011a), and are even consistent with the assumption of a mixture of large smoke particles and Saharan dust (cases 3 and 4). The stronger backscatter wavelength dependence for the 532–1064 nm wavelength range (bsc532/1064), expressed here by an Ångström exponent around 0.8 is also typical for desert dust plumes after leaving the African continent (Tesche et al., 2011a; Haarig et al., 2017a) and reflects the changes in the dust size distribution with a strong decrease of the dust particle number concentration for particles with diameters >5 μm. Examples of size distributions observed with aircraft over Cabo Verde and Barbados during SALTRACE in the June 2013 are given in Weinzierl et al. (2017).

Although the backscatter-related Ångström exponent is usually ≥ 0 for the 355–532 nm wavelength range, in rare cases the Ångström exponent is < 0 as observed in the center of the dust layer on 23 May 2013 (see Fig. 4, case 1, 2–3 km height range). This finding was already discussed by Kanitz et al. (2014). Veselovskii et al. (2016) recently performed lidar measurements of Saharan dust in Senegal and presented several cases with 532 nm backscatter coefficients significantly higher than the ones at 355 nm. This spectral behavior may be caused by a specific chemical composition of the dust particles (and thus specific refractive index characteristics).

The radiosonde profiles of temperature and relative humidity (RH) in Fig. 4 (cases 2-4) are in consistency with the layering structures as observed with lidar and shown in Figs. 2 and 4. The dust layer is drier and warmer (indicated by a strong temperature inversion at SAL base) than the surface-near layers (MBL, MAL). The temperature increased by 6–7 K within 150 m at SAL base in case 2. The less sharp boundary between MAL and SAL (in terms of temperature and RH) in cases 3 and 4 is probably the result of an increasing impact of cloud processes and vertical mixing with increasing travel time over the ocean. The steady increase of the RH with height in the SAL (in cases 1, 3, and 4) indicates well-mixed conditions in the SAL. The RH profile in cases 3 and 4 show a two-layer structure. The lower layer is the cloud-free part of the MBL, the sub-cloud layer (Siebert et al., 2013), and the upper layer is the cloud layer, i.e, in our notation the upper part of the MAL from cloud base of the forming trade wind cumuli up to the trade wind inversion (SAL base).

Figure 6 finally provides an overview of the layer mean optical properties for 532 nm, separately for the MAL and SAL. In 20 nights within the period from 1–23 May, Raman lidar observation over extended time periods of clear skies were possible. Only on 15–16 and 16–17 May continuous occurrence of low level clouds prohibited Raman lidar observations (see Fig. 1, center panel).

Vertical signal smoothing effects close to the layer boundaries are considered in the calculations of the layer mean values by using only data sufficiently above layer base and below layer top. In case of the MAL data analysis, the minimum measurements height was generally set to 400 m. In this way, we avoided a potential bias in the results caused by uncertainties in the correction

of the incomplete laser-beam RFOV overlap. MAL data integration covered the range from 400 to at least 900 m height. Therefore, in cases with MAL top height of <900 m the shown MAL mean values are influenced by dust occurrence (20–23 May period). However, in most cases the MAL (characterized by low depolarization) reached to heights >1000 m (1–19 May period).

5   The findings in Fig. 6 can be summarized as follows: The MAL mean 532 nm backscatter and extinction coefficients vary strongly, from 1–7 Mm^{-1} km^{-1} and 25-150 Mm^{-1}, respectively. This is related to the changing weather and wind-stress conditions which control the amount of sea salt particles in the air. Because of the strong backscatter efficiency of marine particles, the marine backscatter coefficients are typically much larger than the SAL dust backscatter values. Such a strong difference between MAL and SAL data is not visible in the case of the extinction coefficients. The SAL mean extinction
10   values were mostly found between 40 and 100 Mm^{-1} (on average 68±37 Mm^{-1} for all 20 nights). However, during strong dust outbreaks as the 23 May case in Fig. 6b the values can be much higher. A steady decrease of the SAL mean extinction coefficient with travel time is not visible. The SAL (dust + non-dust) AOT in Fig. 6 (bottom panel) ranged from 0.02 to 0.2 over the ocean, more than 1000 km west of the African coast. The 20 night average of the SAL AOT is 0.15±0.13 at 532 nm.

      As in the case of the SAL extinction coefficients, the layer mean lidar ratios (on average 43±8 sr) and depolarization
15   ratios (on average 0.19±0.09) also indicate a travel-time-independent dust characteristics and suggest homogeneous aerosol conditions (regarding particle size spectrum and aerosol mixture) over the Atlantic. A SAL mean particle linear depolarization ratio of 0.17 to 0.25 at 532 nm indicates smoke contributions to the backscatter coefficient of 20% to 50%. In terms of light extinction, the relative smoke contribution is smaller. For a lidar ratio of 30 sr for aged smoke and a lidar ratio of 50 sr for dust, the smoke impact reduces to 10-30% for the extinction coefficients.

20   The ship cruise allowed us also to describe clean marine conditions in terms of lidar specific optical properties at sites far away from continents. The MAL lidar ratios (10-25 sr at 532 nm, mean of 17±5 sr) and depolarization ratios (0.01–0.04, mean of 0.025±0.015) show typical values for clean marine conditions until 19 May (Groß et al., 2011), i.e., when excluding the observations from 20–23 May. The mean MAL extinction coefficient was 67±45 Mm^{-1} for the 1–19 May period.

3.3.1   Conceptual model versus lidar observations (part 2)

25   As mentioned at the end of Sect. 3.2.1 and emphasized in Fig. 3, gravitational settling is responsible for the removal of dust from the SAL in the absence of clouds and precipitation. However, if particle sedimentation would be dominating in the SAL, we should observe a decrease of the coarse dust fraction with height, i.e., an accumulation of the larger dust particles in the lower part of the SAL after dust transport over days and distances of 4000 km and more from Africa (Gasteiger et al., 2017). And this decrease of coarse dust fraction with height should then be reflected in the height profile of the particle depolarization
30   ratio, and other optical parameters such as the particle extinction coefficient and the less noisy backscatter Ångström exponents. As explained in Sect. 2, coarse dust leads to depolarization ratios of 0.35-0.4 at 532 nm, whereas fine dust causes depolarization ratios below 0.2. Thus, according to the conceptual model we should observe a systematic decrease of the depolarization ratio with height in cases 3 and 4 from SAL base to top. But this is not found. No systematic and significant decrease of the

depolarization ratio and of the extinction coefficient and an increase of the backscatter Ångström exponents were observed. Our findings are in agreement with the lidar dust studies over the Atlantic by Yang et al. (2013) and Haarig et al. (2017a).

Furthermore, the measured particle extinction coefficients range from 50–100 Mm^{-1} in the SAL and the dust extinction values between 40 and 80 Mm^{-1} for cases 2–4. Again, a systematic decrease of SAL extinction values with increasing travel time is not observed. Also, no trends in the layer mean values of the lidar ratio and the depolarization ratio in Fig. 6 are visible which would support that size-dependent gravitational settling has strong impact on the dust amount in the SAL and significantly changes the dust size distribution with increasing transport time. All these findings are in agreement with the simulation results of Gasteiger et al. (2017) and the general findings of the SAMUM and SALTRACE campaigns (Weinzierl et al., 2017).

The question is now: what processes can weaken the gravitational settling effect? Gasteiger et al. (2017) argue that absorption of solar radiation introduce turbulent mixing of dust within the SAL and thus upward and downward transport of dust which weakens the pure sedimentation-based dust removal effect. Colarco et. al. (2003) and Yang et al. (2013) discuss the impact of different shapes of dust particles on falling speed and gravitational settling behavior. Ulanowski et al. (2007) observed that dust layers have an impact on the atmospheric electric field, and argue that dust particles can become charged (when colliding with themselves or the underlying surface),and may be vertically aligned in the electric field, and conclude that these charging effect influence the downward transport of dust.

4 Conclusions

During a one-month transatlantic cruise from Guadeloupe to Cabo Verde over 4500 km the aerosol layering structures over the tropical Atlantic were continuously monitored with a multiwavelength lidar aboard the German research vessel R/V Meteor. The lidar allowed us to retrieve a rich set of SAL optical properties during an early summer period in the final phase of the biomass burning season. The absence of anthropogenic particle sources along the transport path over the ocean permitted the study of dust removal aspects in large detail. We investigated to what extend our observations are consistent with the long-range transport features as described by the conceptual model of dust transport and removal over the tropical Atlantic. We found good agreement regarding the aerosol layering structures and the changes in the SAL base and top heights with distance from Africa. We concluded that the removal of dust from the atmosphere below the SAL seems to be much more efficient than expected by the conceptual model. Wet as well as dry deposition controls the removal of dust from the MAL. On the other hand, the observations also suggest a less efficient removal of dust from the SAL than expected, obviously as a consequence of less efficient particle sedimentation. Besides gravitational settling other processes must be active to prolong the lifetime of dust in the SAL. This conclusion was mainly based on the fact that a clear systematic change in the optical properties was not observed, neither with height within the SAL nor with travel time across the Atlantic. The dust extinction coefficient, lidar ratio, and depolarization ratio were fairly constant as function of travel time or distance from Africa.

Regarding the aerosol characteristics we observed that besides desert dust, fire smoke and anthropogenic haze was present in the SAL in May 2013. The SAL vertical mean depolarization of 0.19±0.09 and lidar ratio of 43±8 sr for the May 2013 observational period were clearly lower than the respective values for pure dust of around 0.3 and 55 sr. 80–90% of the 532

nm particle extinction coefficient in the SAL was caused by dust particles in most cases. The further analysis of the SAL lidar ratios suggest that the smoke grew during the long-range transport and changed its backscattering and extinction properties so that the lidar ratio decreased considerably from values around 60 sr (fresh smoke) to values close to 30 sr after a travel time of 5 to 10 days over the tropical Atlantic. Since the conceptual model only covers the summer mode of dust transport, an extension towards including winter mode conditions with complex mixing of dust and smoke at lower altitudes would be desirable.

The shipborne lidar observations in May 2013 fit well into the dust characteristics and layering structures gained from the SAMUM and SALTRACE field campaigns regarding the long range transport of dust. Good agreement regarding the dust optical properties was found when comparing the dust measurements in Morocco, on Cabo Verde, and Barbados, and aboard the R/V Meteor across the Atlantic.

The ship cruise also provided ideal conditions for the measurement of pure marine aerosol optical properties far away from disturbing continents. The results are consistent with the SAMUM-2 observations on Cabo Verde and the winter SALTRACE observations at Barbados. During both campaigns a few days with pure marine conditions occurred. During the ship cruise marine, dust-free conditions in the lowest 1000–1500 m of the atmosphere prevailed continuously for more than two weeks. Typical marine lidar ratios were found to be 15-20 sr at 532 nm. The marine depolarization ratios (controlled by wet sea salt particles) accumulated around 0.03.

In the companion paper Ansmann et al. (2017), the shipborne lidar observations, discussed in this part 1 predominately in terms of dust optical properties, are further analyzed to quantify the fine dust, coarse dust, and non-dust contributions to light extinction and mass concentration by means of the recently introduced POLIPHON method (Mamouri and Ansmann, 2014, 2017). The lidar products are compared with respective forecasts of a regional and two global dust models. Highlight of part 2 is the distinct comparison of observed and modeled fine and coarse dust profiles and thus to focus on aspects regarding the modeled dust size distribution and changes during long-range transport.

The observations in this part 1 and in the follow-up article (part 2) as well as all the advanced lidar observations performed during the dust-related field campaigns in the last 10–15 years clearly indicate the importance and need for comprehensive vertically resolved dust measurements to better understand the life cycle of atmospheric dust, and to improve atmospheric dust modeling from emission to deposition, the interaction of dust with the radiation field, and the dust impact on cloud formation and precipitation. The built-up of a permanent ground-based dust lidar networking infrastructure is mandatory and a clear future task to support dust modeling.

5   Data availability

Radiosondes for measuring, temperature, humidity, and wind profiles were regularly launched at noon and midnight UTC by the German Weather Service (AWI, 2016). GDAS (Global Data Assimilation System) height profiles of temperature and pressure of the National Weather Service's National Centers for Environmental Prediction (NCEP) are used, in addition, for our computations of Rayleigh scattering contributions (NOAA's Air Resources Laboratory ARL, https://www.ready.noaa.gov/gdas1.php) (GDAS, 2016). The shown AOT data are available at *http://aeronet.gsfc.nasa.gov/new_web/cruises_new/Meteor_13_1.html*

(MAN, 2016). The Maritime Aerosol Network (MAN) is a component of AERONET (Smirnov et al., 2009). The trajectories are calculated with the NOAA (National Oceanic and Atmospheric Administration) HYSPLIT (HYbrid Single-Particle Lagrangian Integrated Trajectory) model (http://ready.arl.noaa.gov/HYSPLIT_traj.php) (HYSPLIT, 2016) using GDAS meteorological data (Stein et al., 2015). In addition, fires detected by MODIS (Moderate Resolution Imaging Spectroradiometer)

5   on board the Terra and Aqua satellites are used and are avaialble at http://rapidfire.sci.gsfc.nasa.gov/firemaps (MODIS, 2016). The lidar are available at TROPOS. Please contact Ronny Engelmann (ronny@tropos.de) for further questions.

Acknowledgements. We thank the R/V Meteor team and German Weather Service (DWD) for their support during the cruise M96. We appreciate the effort of AERONET MAN to equip research vessels with sun photometers for atmospheric research.

References

Abdelkader, M., Metzger, S., Mamouri, R. E., Astitha, M., Barrie, L., Levin, Z., and Lelieveld, J.: Dust-air pollution dynamics over the eastern Mediterranean, Atmos. Chem. Phys., 15, 9173-9189, doi:10.5194/acp-15-9173-2015, 2015.

Abdelkader, M., Metzger, S., Steil, B., Klingmüller, K., Tost, H., Pozzer, A., Stenchikov, G., Barrie, L., and Lelieveld, J.: Sensitivity of transatlantic dust transport to chemical aging and related atmospheric processes, Atmos. Chem. Phys., 17, 3799-3821, doi:10.5194/acp-17-3799-2017, 2017.

Adams, A. M., Prospero, J. M., and Zhang, C.: CALIPSO-Derived Three-Dimensional Structure of Aerosol over the Atlantic Basin and Adjacent Continents, J. Climate, 25, 6862-6879, doi:10.1175/jcli-d-11-00672.1, 2012.

Ångström, A.: The Parameters of Atmospheric Turbidity, Tellus, 16, 64–75, 1964.

Ansmann, A., Baars, H., Tesche, M., Müller, D., Althausen, D., Engelmann, R., Pauliquevis, T., and Artaxo, P.: Dust and smoke transport from Africa to South America: Lidar profiling over Cape Verde and the Amazon rainforest, Geophys. Res. Lett., 36, L11802, doi:10.1029/2009GL037923, 2009.

Ansmann, A., Petzold, A., Kandler, K., Tegen, I., Wendisch, M., Müller, D., Weinzierl, B., Müller, T., and Heintzenberg, J.: Saharan mineral dust experiments SAMUM-1 and SAMUM-2: What have we learned?, Tellus B, 63, 403–429, doi:10.1111/j.1600-0889.2011.00555.x, 2011.

Ansmann, A., Seifert, P., Tesche, M., and Wandinger, U.: Profiling of fine and coarse particle mass: case studies of Saharan dust and Eyjafjallajökull/Grimsvötn volcanic plumes, Atmos. Chem. Phys., 12, 9399–9415, doi:10.5194/acp-12-9399-2012, 2012.

Ansmann, A., Rittmeister, F., Engelmann, R., Basart, S., Benedetti, A., Spyrou, C., Skupin, A., Baars, H., Seifert, P., and Kanitz, T.: Profiling of Saharan dust from the Caribbean to West Africa, Part 2: Shipborne lidar measurements versus dust forecasts, Atmos. Chem. Phys., SALTRACE special issue, in preparation, 2017.

Atkinson, J. D., Murray, B. J., Woodhouse, M. T., Whale, T. F., Baustian, K. J., Carslaw, K. S., Dobbie, S., O'Sullivan, D., and Malkin, T. L.: The importance of feldspar for ice nucleation by mineral dust in mixed-phase clouds, Nature, 498, 355–358, doi:10.1038/nature12278, 2013.

AWI: Pangaea data base, available at: https://www.pangaea.de/, last access: October, 2016.

Baars, H., Ansmann, A., Engelmann, R., and Althausen, D.: Continuous monitoring of the boundary-layer top with lidar, Atmos. Chem. Phys., 8, 7281-7296, doi:10.5194/acp-8-7281-2008, 2008.

Baars, H., Ansmann, A., Althausen, D., Engelmann, R., Artaxo, P., Pauliquevis, T., and Souza, R.: Further evidence for significant smoke transport from Africa to Amazonia, Geophys. Res. Lett., 38, L20802, doi:10.1029/2011GL049200, 2011.

Baars, H., Kanitz, T., Engelmann, R., Althausen, D., Heese, B., Komppula, M., Preißler, J., Tesche, M., Ansmann, A., Wandinger, U., Lim, J.-H., Ahn, J. Y., Stachlewska, I. S., Amiridis, V., Marinou, E., Seifert, P., Hofer, J., Skupin, A., Schneider, F., Bohlmann, S., Foth, A., Bley, S., Pfüller, A., Giannakaki, E., Lihavainen, H., Viisanen, Y., Hooda, R. K., Pereira, S. N., Bortoli, D., Wagner, F., Mattis, I., Janicka, L., Markowicz, K. M., Achtert, P., Artaxo, P., Pauliquevis, T., Souza, R. A. F., Sharma, V. P., van Zyl, P. G., Beukes, J. P., Sun, J., Rohwer, E. G., Deng, R., Mamouri, R.-E., and Zamorano, F.: An overview of the first decade of PollyNET: an emerging network of automated Raman-polarization lidars for continuous aerosol profiling, Atmos. Chem. Phys., 16, 5111-5137, doi:10.5194/acp-16-5111-2016, 2016.

Balkanski, Y., Schulz, M., Claquin, T., and Guibert, S.: Reevaluation of Mineral aerosol radiative forcings suggests a better agreement with satellite and AERONET data, Atmos. Chem. Phys., 7, 81-95, doi:10.5194/acp-7-81-2007, 2007.

Ben-Ami, Y., Koren, I., and Altaratz, O.: Patterns of North African dust transport over the Atlantic: winter vs. summer, based on CALIPSO first year data, Atmos. Chem. Phys., 9, 7867-7875, doi:10.5194/acp-9-7867-2009, 2009.

Ben-Ami, Y., Koren, I., Rudich, Y., Artaxo, P., Martin, S. T., and Andreae, M. O.: Transport of North African dust from the Bodélé depression to the Amazon Basin: a case study, Atmos. Chem. Phys., 10, 7533-7544, doi:10.5194/acp-10-7533-2010, 2010.

5   Cakmur, R. V., Miller, R. L., Perlwitz, J., Geogdzhayev, I. V., Ginoux, P., Koch, D., Kohfeld, K. E., Tegen, I., and Zender, C. S.: Constraining the magnitude of the global dust cycle by minimizing the difference between amodel and observations, J. Geophys. Res. 111, D06207, doi:10.1029/2005JD005791, 2006.

Colarco, P. R., Toon, O. B., Reid, J. S., Livingston, J. M., Russell, P. B., Redemann, J., Schmid, B., Maring, H. B., Savoie, D., Welton, E. J., Campbell, J. R., Holben, B. N., and Levy, R.: Saharan dust transport to the Caribbean during PRIDE: 2. Transport, vertical profiles,

10 and deposition in simulations of in situ and remote sensing observations, J. Geophys. Res., 108, 8590, doi:10.1029/2002JD002659, D19, 2003.

Dawson, K. W., Meskhidze, N., Josset, D., and Gassó, S.: Spaceborne observations of the lidar ratio of marine aerosols, Atmos. Chem. Phys., 15, 3241-3255, https://doi.org/10.5194/acp-15-3241-2015, 2015.

DeMott, P. J., Prenni, A. J., McMeeking, G. R., Sullivan, R. C., Petters, M. D., Tobo, Y., Niemand, M., Möhler, O., Snider, J. R., Wang, Z.,

15 and Kreidenweis, S. M.: Integrating laboratory and field data to quantify the immersion freezing ice nucleation activity of mineral dust particles, Atmos. Chem. Phys., 15, 393-409, doi:10.5194/acp-15-393-2015, 2015.

Denjean, C., Caquineau, S., Desboeufs, K., Laurent, B., Maille, M., Quiñones Rosado, M., Vallejo, P., Mayol-Bracero, O. L., and Formenti, P.: Long-range transport across the Atlantic in summertime does not enhance the hygroscopicity of African mineral dust, Geophys. Res. Lett., 42, 7835–7843, doi:10.1002/2015GL065693, 2015.

20 Engelmann, R., Ansmann, A., Fruntke, J., Seifert, P., Tesche, M., Althausen, D., Müller, D., Esselborn, M., Lieke, K., and Köhler, C.: Doppler lidar observations of heat–island effects on vertical mixing of dust and smoke over Cape Verde during SAMUM–2, Tellus B, 63, 448–458, doi:10.1111/j.1600-0889.2011.00552.x, 2011.

Engelmann, R., Kanitz, T., Baars, H., Heese, B., Althausen, D., Skupin, A., Wandinger, U., Komppula, M., Stachlewska, I. S., Amiridis, V., Marinou, E., Mattis, I., Linné, H., and Ansmann, A.: The automated multiwavelength Raman polarization and water-vapor lidar PollyXT:

25 the neXT generation, Atmos. Meas. Tech., 9, 1767-1784, doi:10.5194/amt-9-1767-2016, 2016.

Franke, K., Ansmann, A., Müller, D., Althausen, D., Venkataraman, C., Reddy, M. S., Wagner, F., and Scheele, R.: Optical properties of the Indo–Asian haze layer over the tropical Indian Ocean, J. Geophys. Res., 108, 4059, doi:10.1029/2002JD002473, 2003.

Freudenthaler, V., Esselborn, M., Wiegner, M., Heese, B., Tesche, M., Ansmann, A., Müller, D., Althausen, D., Wirth, M., Fix, A., Ehret, G., Knippertz, P., Toledano, C., Gasteiger, J., Garhammer, M., and Seefeldner, M.: Depolarization ratio profiling at several wavelengths in

30 pure Saharan dust during SAMUM 2006, Tellus B, 61, 165–179. doi: 10.1111/j.1600-0889.2008.00396.x, 2009.

Gasteiger, J., Groß, S., Sauer, D., Haarig, M., Ansmann, A., and Weinzierl, B.: Particle settling and vertical mixing in the Saharan Air Layer as seen from an integrated model, lidar, and in situ perspective, Atmos. Chem. Phys., 17, 297-311, doi:10.5194/acp-17-297-2017, 2017.

GDAS: Global Data Assimilation System, meteorological data base, available at: https://www.ready.noaa.gov/gdas1.php, last access: October, 2016.

35 Groß, S., Tesche, M., Freudenthaler, V., Toledano, C., Wiegner, M., Ansmann, A., Althausen, D., and Seefeldner, M.: Characterization of Saharan dust, marine aerosols and mixtures of biomass-burning aerosols and dust by means of multi-wavelength depolarization and Raman lidar measurements during SAMUM 2, Tellus B, 63, 706-724, doi:10.1111/j.1600-0889.2011.00556.x, 2011.

Groß, S., Freudenthaler, V., Schepanski, K., Toledano, C., Schäfler, A., Ansmann, A., and Weinzierl, B.: Optical properties of long-range transported Saharan dust over Barbados as measured by dual-wavelength depolarization Raman lidar measurements, Atmos. Chem. Phys., 15, 11067-11080, doi:10.5194/acp-15-11067-2015, 2015.

Groß, S., Gasteiger, J., Freudenthaler, V., Müller, T., Sauer, D., Toledano, C., and Ansmann, A.: Saharan dust contribution to the Caribbean summertime boundary layer - a lidar study during SALTRACE, Atmos. Chem. Phys., 16, 11535-11546, doi:10.5194/acp-16-11535-2016, 2016.

Haarig, M., Althausen, D., Ansmann, A., Klepel, A., Baars, H., Engelmann, R., Groß, S., and Freudenthaler, V.: Measurement of the linear depolarization ratio of aged dust at three wavelengths (355, 532 and 1064 nm) simultaneously over Barbados, EPJ Web of Conferences, 119, 18009, ILRC 27, DOI: 10.1051/epjconf/201611918009, 2016.

Haarig, M., Ansmann, A., Althausen, D., Klepel, A., Groß, S., Freudenthaler, V., Toledano, C., Mamouri, R.-E., Farrell, D. A., Prescod, D. A., Marinou, E., Burton, S. P., Gasteiger, J., Engelmann, R., and Baars, H.: Triple-wavelength depolarization-ratio profiling of Saharan dust over Barbados during SALTRACE in 2013 and 2014, Atmos. Chem. Phys. Discuss., doi:10.5194/acp-2017-170, in review, 2017.

Haarig, M., Ansmann, A., Gasteiger, J., Kandler, K., Althausen, D., Baars, H., and , Farrell, D.: Dry versus wet marine particle optical properties: RH dependence of depolarization ratio, backscatter and extinction from multiwavelength lidar measurements during SALTRACE, Atmos. Chem. Phys. Discuss., doi:10.5194/acp-2017-545, in review, 2017b.

Heintzenberg, J.: The SAMUM–1 experiment over Southern Morocco: Overview and introduction, Tellus B, 61, 2-11, doi:10.1111/j.1600-0889.2008.00403.x, 2009.

Hofer, J., Althausen, D., Abdullaev, S. F., Engelmann, R., and Baars, H.: Central Asian Dust Experiment (CADEX): Multiwavelength Polarization Raman Lidar Observations in Tajikistan, EPJ Web of Conferences, 119, 18006, ILRC 27, DOI: 10.1051/epjconf/201611918006, 2016.

Hofer, J., Althausen, D., Abdullaev, S. F., Makhmudov, A., Nazarov, B. I., Schettler, G., Engelmann, R., Baars, H., Fomba, K. W., Müller, K., Heinold, B., Kandler, K., and Ansmann, A.: Long-term profiling of mineral dust and pollution aerosol with multiwavelength polarization Raman lidar at the central Asian site of Dushanbe Tajikistan: Case studies, Atmos. Chem. Phys., doi:10.5194/acp-2017-559, in review, 2017.

Hoose, C. and Möhler, O.: Heterogeneous ice nucleation on atmospheric aerosols: a review of results from laboratory experiments, Atmos. Chem. Phys., 12, 9817-9854, doi:10.5194/acp-12-9817-2012, 2012

Huneeus, N., Schulz, M., Balkanski, Y., Griesfeller, J., Prospero, J., Kinne, S., Bauer, S., Boucher, O., Chin, M., Dentener, F., Diehl, T., Easter, R., Fillmore, D., Ghan, S., Ginoux, P., Grini, A., Horowitz, L., Koch, D., Krol, M. C., Landing, W., Liu, X., Mahowald, N., Miller, R., Morcrette, J.-J., Myhre, G., Penner, J., Perlwitz, J., Stier, P., Takemura, T., and Zender, C. S.: Global dust model intercomparison in AeroCom phase I, Atmos. Chem. Phys., 11, 7781-7816, doi:10.5194/acp-11-7781-2011, 2011.

HYSPLIT: HYbrid Single-Particle Lagrangian Integrated Trajectory model, backward trajectory calculation tool, available at: http://ready.arl.noaa.gov/HYSPLIT_traj.php, last access: October, 2016.

Jähn, M., Muñoz-Esparza, D., Chouza, F., Reitebuch, O., Knoth, O., Haarig, M., and Ansmann, A.: Investigations of boundary layer structure, cloud characteristics and vertical mixing of aerosols at Barbados with large eddy simulations, Atmos. Chem. Phys., 16, 651-674, doi:10.5194/acp-16-651-2016, 2016.

Kanitz, T., Seifert, P., Ansmann, A., Engelmann, R., Althausen, D., Casiccia, C., and Rohwer, E. G.: Contrasting the impact of aerosols at northern and southern midlatitudes on heterogeneous ice formation, Geophys. Res. Lett., 38, L17802, doi:10.1029/2011GL048532, 2011.

Kanitz, T., Ansmann, A., Seifert, P., Engelmann, R., Kalisch, J., and Althausen, D.: Radiative effect of aerosols above the northern and southern Atlantic Ocean as determined from shipborne lidar observations, J. Geophys. Res. Atmos., 118, 12,556–12,565, doi:10.1002/2013JD019750, 2013.

Kanitz, T., Engelmann, R., Heinold, B., Baars, H., Skupin, A., and Ansmann, A.: Tracking the Saharan Air Layer with shipborne lidar across the tropical Atlantic, Geophys. Res. Lett., 41, 1044–1050, doi:10.1002/2013GL058780, 2014.

Karyampudi, V. M., Palm, S. P., Reagen, J. A., Fang, H., Grant, W. B., Hoff, R. M., Moulin, C., Pierce, H. F., Torres, O., Browell, E. V., Melfi, S. H.: Validation of the Saharan Dust Plume Conceptual Model Using Lidar, Meteosat, and ECMWF Data, Bull. Amer. Meteor. Soc., 80, 1045–1075, doi:10.1175/1520-0477(1999)080<1045:VOTSDP>2.0.CO;2, 1999.

Kiselev, A., Bachmann, F., Pedevilla, P., Cox, S. J., Michaelides, A., Gerthsen, D., and Leisner, T.: Active sites in heterogeneous ice nucleation—the example of K-rich feldspars, Science, 355, 367–371, doi: 10.1126/science.aai8034, 2017.

Liu, D., Wang, Z., Liu, Z., Winker, D., and Trepte, C.: A height resolved global view of dust aerosols from the first year CALIPSO lidar measurements, J. Geophys. Res., 113, D16214, doi:10.1029/2007JD009776, 2008a.

Liu, Z., Omar, A., Vaughan, M., Hair, J., Kittaka, C., Hu, Y., Powell, K., Trepte, C., Winker, D., Hostetler, C., Ferrare, R., and Pierce, R.: CALIPSO lidar observations of the optical properties of Saharan dust: A case study of long-range transport, J. Geophys. Res., 113, D07207, doi:10.1029/2007JD008878, 2008b.

Mamouri, R. E. and Ansmann, A.: Fine and coarse dust separation with polarization lidar, Atmos. Meas. Tech., 7, 3717-3735, doi:10.5194/amt-7-3717-2014, 2014.

Mamouri, R. E. and Ansmann, A.: Estimated desert-dust ice nuclei profiles from polarization lidar: methodology and case studies, Atmos. Chem. Phys., 15, 3463-3477, doi:10.5194/acp-15-3463-2015, 2015.

Mamouri, R.-E. and Ansmann, A.: Potential of polarization/Raman lidar to separate fine dust, coarse dust, maritime, and anthropogenic aerosol profiles, Atmos. Meas. Tech. Discuss., doi:10.5194/amt-2017-131, in review, 2017.

MAN: Maritime Aerosolo Network: MAN aerosol data base, available at: http://aeronet.gsfc.nasa.gov/new_web/cruises_new/Meteor_13_1.html, last access: October, 2016.

McCormick, M. P., Winker, D. M., Browell, E. V., Coakley, J. A., Gardner, C. S., Hoff, R. M., Kent, G. S., Melfi, S. H., Menzies, R. T., Platt, C. M. R., Randall, D. A., and Reagan, J. A.: Scientific Investigations Planned for the Lidar In-Space Technology Experiment (LITE). Bull. Amer. Meteor. Soc., 74, 205–214, doi: http://dx.doi.org/10.1175/1520-0477(1993)074<0205:SIPFTL>2.0.CO;2, 1993.

MODIS: MODIS fire information, available at: http://rapidfire.sci.gsfc.nasa.gov/firemaps, last access: October, 2016.

Müller, D., Mattis, I., Wandinger, U., Ansmann, A., Althausen, A., and Stohl, A.: Raman lidar observations of aged Siberian and Canadian forest fire smoke in the free troposphere over Germany in 2003: Microphysical particle characterization, J. Geophys. Res., 110, D17201, doi:10.1029/2004JD005756, 2005.

Müller, D., Mattis, I., Ansmann, A., Wandinger, U., Ritter, C., and Kaiser, D.: Multiwavelength Raman lidar observations of particle growth during long-range transport of forest-fire smoke in the free troposphere, Geophys. Res. Lett., 34, L05803, doi:10.1029/2006GL027936, 2007a.

Müller, D., Ansmann, A., Mattis, I., Tesche, M., Wandinger, U., Althausen, D., and Pisani, G.: Aerosol-type-dependent lidar ratios observed with Raman lidar, J. Geophys. Res., 112, D16202, doi:10.1029/2006JD008292, 2007b.

Murray, B. J., O'Sullivan, D., Atkinson, J. D., and Webb, M. E.: Ice nucleation by particles immersed in supercooled cloud droplets, Chem. Soc. Rev., 41, 6519-6554, doi:10.1039/c2cs35200a, 2012.

Myhre, G. and Stordal, F.: Global sensitivity experiments of the radiative forcing due to mineral aerosols, J. Geophys. Res. 106, 18193-18204, doi:10.1029/2000JD900536, 2001.

Nikonovas, T., North, P. R. J., and Doerr, S. H.: Smoke aerosol properties and ageing effects for northern temperate and boreal regions derived from AERONET source and age attribution, Atmos. Chem. Phys., 15, 7929-7943, doi:10.5194/acp-15-7929-2015, 2015.

Osborne, S. R., Johnson, B. T., Haywood, J. M., Baran, A. J., Harrison, M. A. J., and McConnell, C. L.: Physical and optical properties of mineral dust aerosol during the Dust and Biomass-burning Experiment, J. Geophys. Res., 113, D00C03, doi:10.1029/2007JD009551, 2008.

Prospero, J. M.: Atmospheric dust studies on Barbados, Bull. Amer. Meteorol. Soc., 49, 645-652, 1968.

Prospero, J. M., and Carlson, T. N.: Vertical and areal distribution of Saharan dust over the western equatorial North Atlantic Ocean, J. Geophys. Res., 77, 5255-5265, 1972

Prospero, J. M., Ginoux, P., Torres, O., Nicholson, S. E. and Gill, T. E.: Environmental characterization of global sources of atmospheric soil dust identified with the Nimbus 7 Total Ozone Mapping Spectrometer (TOMS) absorbing aerosol product, Rev. Geophys. 40, doi:10.1029/2000RG000095, 2002.

Rittmeister, F.: The African dust and smoke layer over the tropical Atlantic during the spring season of 2013: Ship-based lidar observations from Guadeloupe to Cape Verde, University Master Thesis, 69 pages, Universität Leipzig, Germany, 2015.

Ryder, C. L., McQuaid, J. B., Flamant, C., Rosenberg, P. D., Washington, R., Brindley, H. E., Highwood, E. J., Marsham, J. H., Parker, D. J., Todd, M. C., Banks, J. R., Brooke, J. K., Engelstaedter, S., Estelles, V., Formenti, P., Garcia-Carreras, L., Kocha, C., Marenco, F., Sodemann, H., Allen, C. J. T., Bourdon, A., Bart, M., Cavazos-Guerra, C., Chevaillier, S., Crosier, J., Darbyshire, E., Dean, A. R., Dorsey, J. R., Kent, J., O'Sullivan, D., Schepanski, K., Szpek, K., Trembath, J., and Woolley, A.: Advances in understanding mineral dust and boundary layer processes over the Sahara from Fennec aircraft observations, Atmos. Chem. Phys., 15, 8479-8520, doi:10.5194/acp-15-8479-2015, 2015.

Phillips, V. T. J., DeMott, P. J., Andronache, C., Pratt, K. A., Prather, K. A., Subramanian, R., and Twohy, C.: Improvements to an empirical parameterization of heterogeneous ice nucleation and its comparison with observations, J. Atmos. Sci., 70, 378-409, doi:10.1175/JAS-D-12-080.1, 2013

Schepanski, K., Tegen, I., and Macke, A.: Saharan dust transport and deposition towards the tropical northern Atlantic, Atmos. Chem. Phys., 9, 1173-1189, doi:10.5194/acp-9-1173-2009, 2009.

Seifert, P., Ansmann, A., Mattis, I., Wandinger, U., Tesche, M., Engelmann, R., Müller, D., Pérez, C., and Haustein, K.: Saharan dust and heterogeneous ice formation: eleven years of cloud observations at a central European EARLINET site, J. Geophys. Res., 115, D20201, doi:10.1029/2009JD013222, 2010.

Shimizu, A., Sugimoto, N., Matsui, I., Arao, K., Uno, I., Murayama, T., Kagawa, N., Aoki, K., Uchiyama, A., and Yamazaki, A.: Continuous observations of Asian dust and other aerosols by polarization lidars in China and Japan during ACE-Asia, J. Geophys. Res., 109, D19S17, doi:10.1029/2002JD003253, 2004.

Siebert, H., Beals, M., Bethke, J., Bierwirth, E., Conrath, T., Dieckmann, K., Ditas, F., Ehrlich, A., Farrell, D., Hartmann, S., Izaguirre, M. A., Katzwinkel, J., Nuijens, L., Roberts, G., Schäfer, M., Shaw, R. A., Schmeissner, T., Serikov, I., Stevens, B., Stratmann, F., Wehner, B., Wendisch, M., Werner, F., and Wex, H.: The fine-scale structure of the trade wind cumuli over Barbados - an introduction to the CARRIBA project, Atmos. Chem. Phys., 13, 10061-10077, doi:10.5194/acp-13-10061-2013, 2013.

Smirnov, A., Holben, B. N., Slutsker, I., Giles, D. M. McClain, C. R., Eck, T. F., Sakerin, S. M., Macke, A., Croot, P., Zibordi, G., Quinn, P. K., Sciare, J., Kinne, S., Harvey, M., Smyth, T. J., Piketh, S., Zielinski, T., Proshutinsky, A., Goes, J. I., Nelson, N. B., Larouche,

P., Radionov, V. F., Goloub, P., Krishna Moorthy, K., Matarrese, R., Robertson, E. J., and Jourdin, F.: Maritime Aerosol Network as a component of Aerosol Robotic Network, J. Geophys. Res., 114, D06204, doi:10.1029/2008JD011257, 2009.

Sokolik, I. N., Winker, D. M., Bergametti, G., Gillette, D. A., Carmichael, G., Kaufman, Y. J., Gomes, L., Schütz, L., and Penner, J. E.: Introduction to special section: Outstanding problems in quantifying the radiative impacts of mineral dust, J. Geophys. Res., 106, 18015-18028, doi:10.1029/2000JD900498, 2001.

Stein, A. F., Draxler, R. R., Rolph, G. D., Stunder, B. J. B., Cohen, M. D., and Ngan, F.: NOAA's HYSPLIT Atmospheric Transport and Dispersion Modeling System. Bull. Amer. Meteorol. Soc., 96, 2059–2077, doi: 10.1175/BAMS-D-14-00110.1, 2015

Sugimoto, N., Uno, I., Nishikawa, M., Shimizu, A., Matsui, I., Dong, X., Chen, Y., and Quan, H.: Record heavy Asian dust in Beijing in 2002: Observations and model analysis of recent events. Geophys. Res. Lett., 30, 1640, doi:10.1029/2002GL016349, 2003.

Tegen, I.: Modeling the mineral dust aerosol cycle in the climate system, Quat. Sci. Rev., 22, 1821-1834, doi:10.1016/S0277-3791(03)00163-X, 2003.

Tesche, M., Ansmann, A., Müller, D., Althausen, D., Engelmann, R., Freudenthaler, V., and Groß, S.: Vertically resolved separation of dust and smoke over Cape Verde using multiwavelength Raman and polarization lidars during Saharan Mineral Dust Experiment 2008, J. Geophys. Res., 114, D13202, doi:10.1029/2009JD011862, 2009.

Tesche, M., Groß, S., Ansmann, A., Müller, D., Althausen, D., Freudenthaler, V., and Esselborn, M.: Profiling of Saharan dust and biomass-burning smoke with multiwavelength polarization Raman lidar at Cape Verde, Tellus B, 63, 649–676, doi:10.1111/j.1600-0889.2011.00548.x, 2011a.

Tesche, M., Müller, D., Groß, S., Ansmann, A., Althausen, D., Freudenthaler, V., Weinzierl, B., Veira, A., and Petzold, A.: Optical and microphysical properties of smoke over Cape Verde inferred from multiwavelength lidar measurements. Tellus B, 63, 677–694. doi:10.1111/j.1600-0889.2011.00549.x, 2011b.

Tsamalis, C., Chédin, A., Pelon, J., and Capelle, V.: The seasonal vertical distribution of the Saharan Air Layer and its modulation by the wind, Atmos. Chem. Phys., 13, 11235-11257, doi:10.5194/acp-13-11235-2013, 2013.

Ulanowski, Z., Bailey, J., Lucas, P. W., Hough, J. H., and Hirst, E.: Alignment of atmospheric mineral dust due to electric field, Atmos. Chem. Phys., 7, 6161-6173, doi:10.5194/acp-7-6161-2007, 2007.

Veselovskii, I., Goloub, P., Podvin, T., Bovchaliuk, V., Derimian, Y., Augustin, P., Fourmentin, M., Tanré, D., Korenskiy, M., Whiteman, D. N., Diallo, A., Ndiaye, T., Kolgotin, A., and Dubovik, O.: Retrieval of optical and physical properties of African dust from multiwavelength Raman lidar measurements during the SHADOW campaign in Senegal, Atmos. Chem. Phys., 16, 7013-7028, doi:10.5194/acp-16-7013-2016, 2016.

Weinzierl, B., Ansmann, A, Prospero, J. M., Althausen, D., Benker, N., Chouza, F., Dollner, M., Farrell, D., Fomba, W. K., Freudenthaler, V., Gasteiger, J., Groß, S., Haarig, M., Heinold, B., Kandler, K., Kristensen, T. B., Mayol-Bracero, O.-L., Müller, T., Reitebuch, O., Sauer, D., Schäfler, A., Schepanski, K., Spanu, A., Tegen, I., Toledano, C., Walser, A.: The Saharan Aerosol Long-range TRansport and Aerosol Cloud Interaction Experiment (SALTRACE): overview and selected highlights, Bull. Amer. Meteorol. Soc., doi:10.1175/BAMS-D-15-00142.1, in press, 2017.

Yang, W., Marshak, A., Kostinski, A. B., and Várnai, T.: Shape-induced gravitational sorting of Saharan dust during transatlantic voyage: Evidence from CALIOP lidar depolarization measurements, Geophys. Res. Lett., 40, 3281–3286, doi:10.1002/grl.50603, 2013.
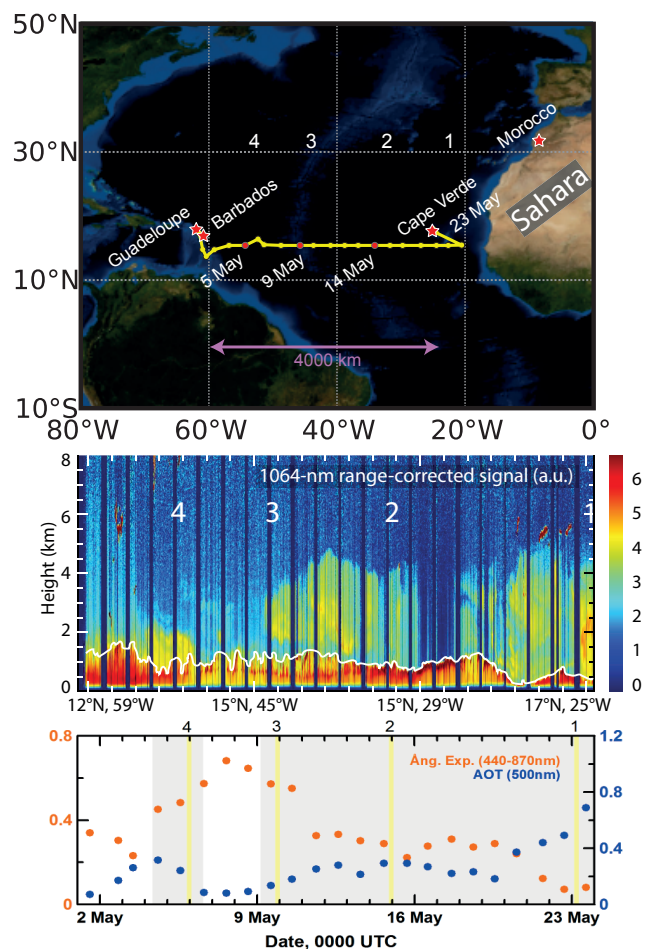
Figure 1. (Top) Cruise track of the R/V Meteor from Guadeloupe (29 April 2013) to Cape Verde (23 May 2013) plotted as a thick yellow line (Kanitz et al., 2014). The SAMUM-1 (Morocco), SAMUM-2 (Cape Verde), and SALTRACE (Barbados) field sites are marked by red stars. Red circles and dates (5, 9, 14 and 23 May) indicate the locations of four lidar observations (cases 1, 2, 3, and 4) discussed in detail in this paper and the follow-up article. (Center) Dust-free marine aerosol layer (MAL, top height as a white line) and lofted Saharan air layer (SAL). The composite is based on lidar measurements of the range-corrected 1064 nm backscatter signal. Measurement breaks around 1200 local time (dark vertical lines) are due to high sun elevation and shut down of the lidar. (Bottom) Time series of daily mean sun photometer observations of aerosol optical thickness (AOT) (blue circles) and Ångström exponent (orange circles). The gray-shaded areas indicate time periods with lofted dust. The yellow vertical lines indicate the selected four observational cases.
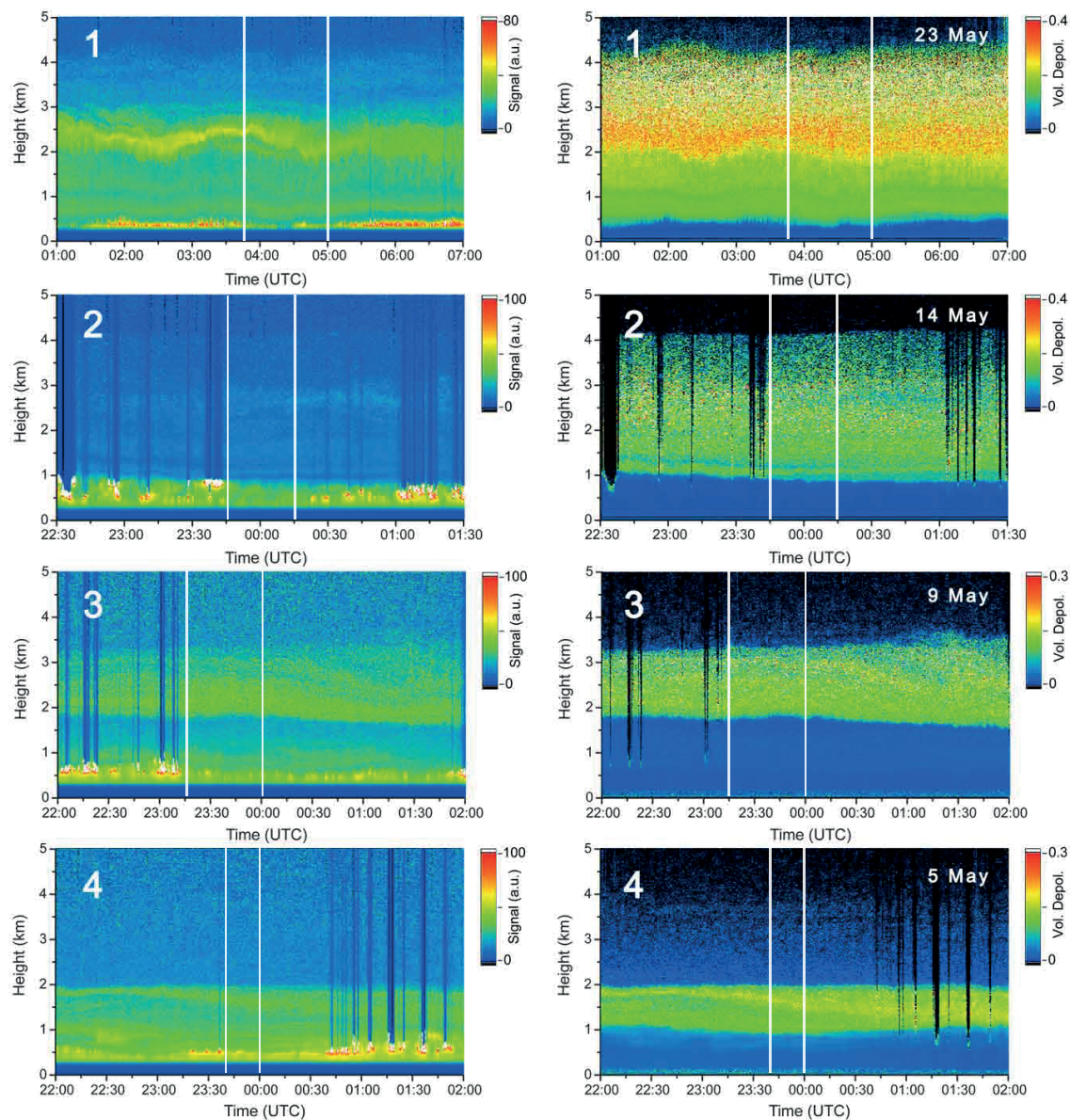
Figure 2. Marine and dust layers over the tropical Atlantic about 1000 km (1), 1700 km (2), 3300 km (3), 4300 km (4) west of the African coast. The 532 nm range-corrected signal (left) and 532 nm volume linear depolarization ratio (right) are shown. Linear color scale is used. Temporal and vertical resolution is 30 s and 7.5 m, respectively. The SAL is on top of the MAL (given in blue in the right panels). White spots in the left panels (below 1 km) indicate trade wind cumuli close to the top of the MBL, the convective part of the MAL. Vertical lines indicate the signal averaging periods for which profiles of optical properties are discussed in Sect. 3.3. Lidar overlap effects (lowest 250 m) prohibit a clear aerosol detection in the near-range of the lidar in the left panels.
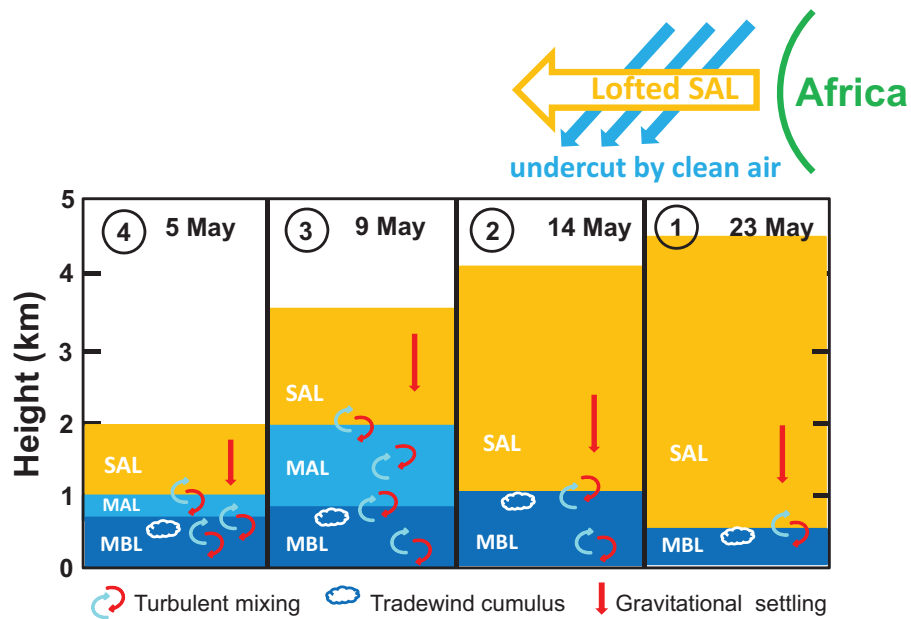
Figure 3. (Top) Sketch of the east-to-west dust transport in the lofted SAL which is undercut by clean trade winds from the Northeast (occurring in the MAL) according to the dust plume conceptual model of Karyampudi et al. (1999), described in Sect. 1.1. (Bottom) Sketch of dust layering (SAL in orange, MAL and its convective part MBL in blue). Base and top heights of the MBL, MAL, and SAL are taken from Fig. 2. Gravitational settling (symbolized by a red arrow) is responsible for the removal of dust from the SAL, turbulent downward mixing (symbolized by curved arrows) plays an important role in the removal of dust from the MAL.

.
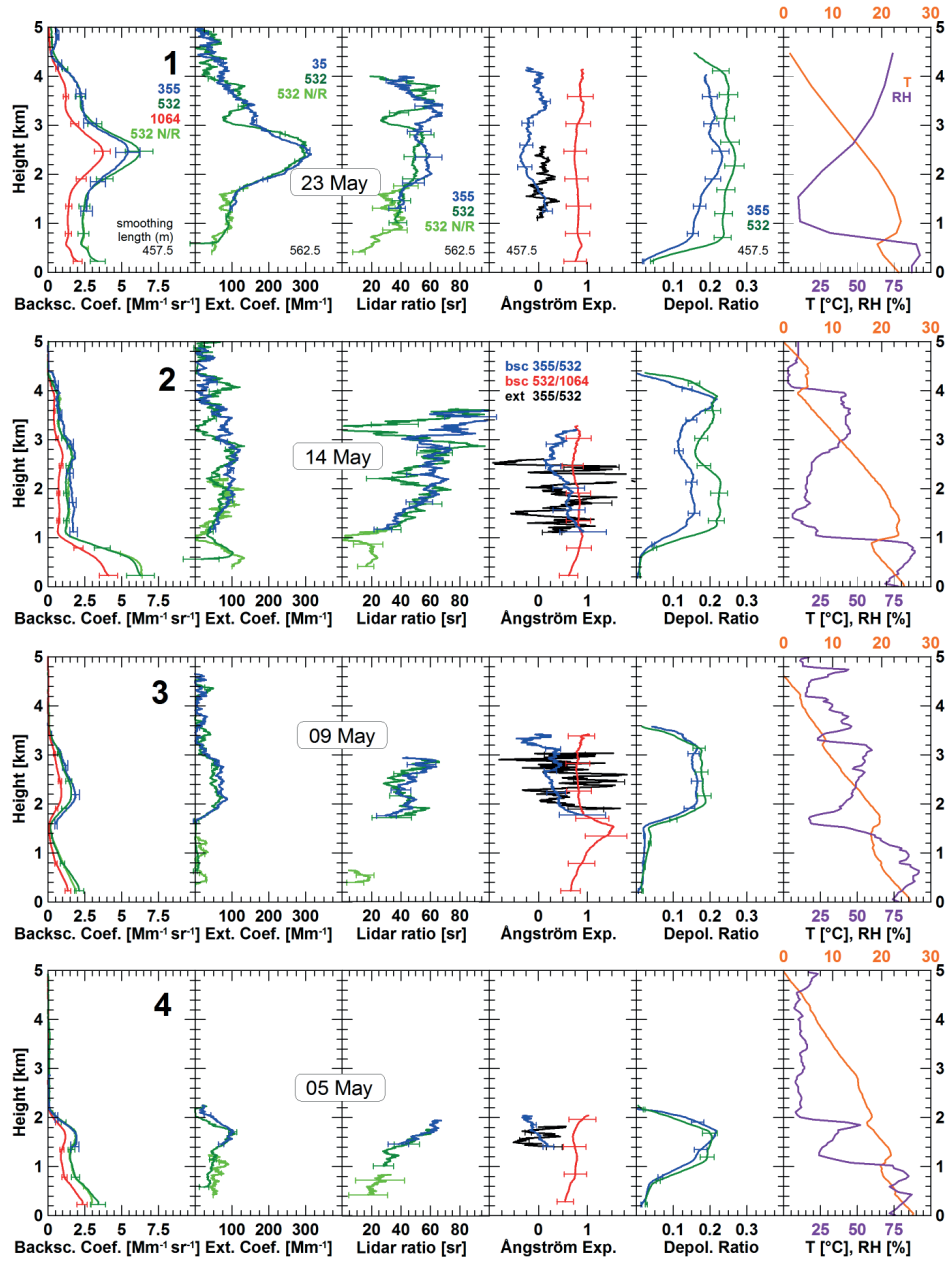
Figure 4. Profiles of the particle backscatter coefficient at 355, 532, and 1064 nm, extinction coefficient, extinction-to-backscatter ratio (lidar ratio), and particle linear depolarization ratio at 355 and 532 nm, and backscatter-related (bsc) and extinction-related (ext) Ångström exponents. Temperature and relative humidity (from radiosonde, except 23 May, GDAS) are given in addition. Mean profiles of the optical properties for the time periods on 23 May 2013, 03:45–05:00 UTC (case 1), 14–15 May 2013, 23:45–00:15 UTC (case 2), 9 May 2013, 23:15–24:00 UTC (case 3), and 5 May 2013, 23:40–24:00 UTC (case 4) are shown. The label 532 N/R denotes the 532 nm near-range receiver channel. The vertical signal smoothing length for the profiles of backscatter coefficient and particle linear depolarization ratio is 457.5 m, the rest is smoothed with 562.5 m window length. The signal averaging periods are indicated by white vertical lines in Fig. 2.
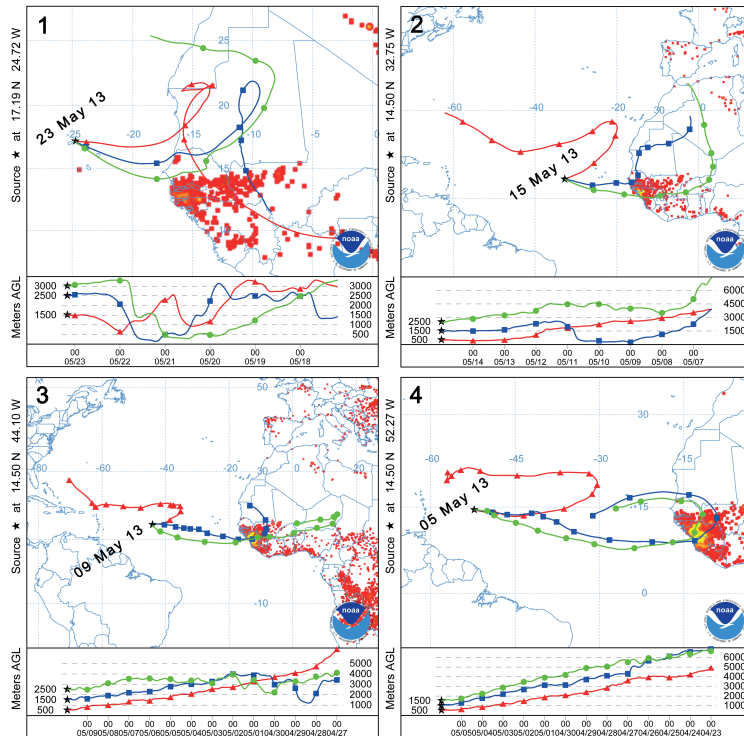
Figure 5. Five-day to 13-day HYSPLIT backward trajectories for 23 May 2013, 04:00 UTC (case 1), 15 May 2013, 00:00 UTC (case 2), 9 May 2013, 23:00 UTC (case 3), and 5 May 2013, 23:00 UTC (case 4). Symbols indicate air mass transport from day to day. The arrival height level of 500 m (red) is in the MAL. Arrival heights of 1500–3000 m (blue, green) are in the SAL. In addition, fires (red dotes) detected by MODIS on board the Terra and Aqua satellites are shown accumulated over a 10-day period each (21–30 April 2013 for cases 3 and 4, 11–20 May 2013 for case 2, and 21–30 May 2013 for case 1).
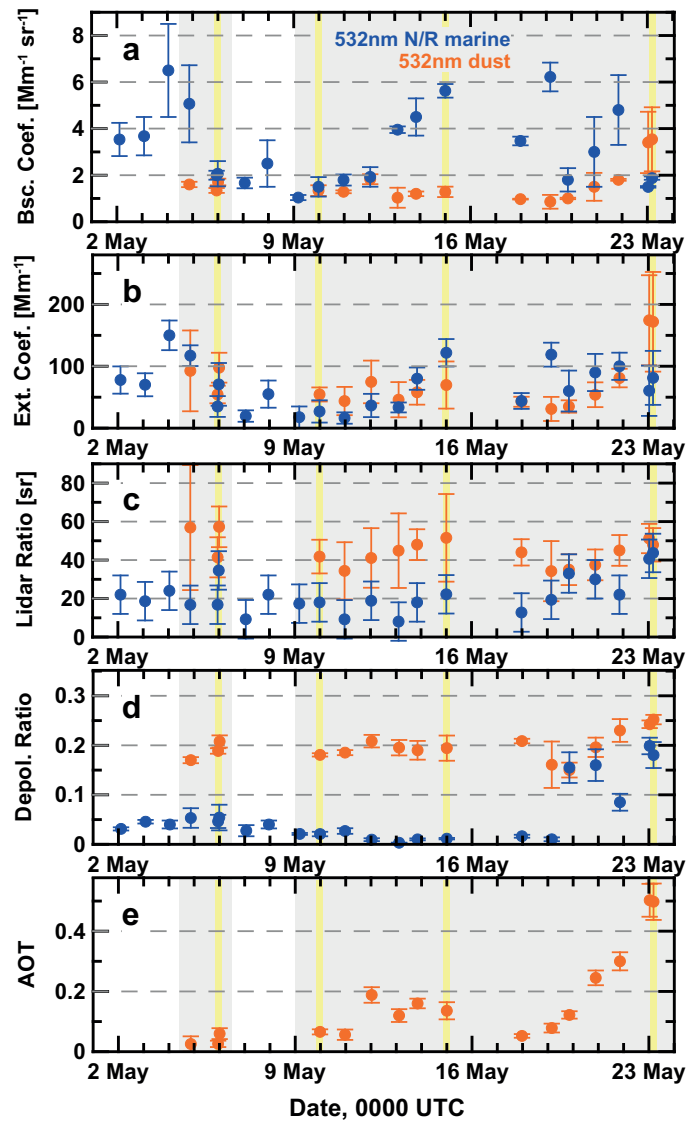
Figure 6. MAL (blue) and SAL (red) vertical mean values of (a) 532 nm particle backscatter coefficient, (b) extinction coefficient, (c) lidar ratio, and (d) linear depolarization ratio observed with lidar in 20 nights in May 2013. 30–120 minute averages are shown. Cases 1–4 are indicated as vertical yellow lines. The SAL AOT at 532 nm is given in panel e. Error bars (one standard deviation) indicate the retrieval uncertainty and atmospheric variability within the analyzed layers. The two periods with dust are shown as gray areas.